Evaluation of Normalisation Methods for Uniaxial Bias Extension Tests on Engineering Fabrics

F. Härtel[a] and P. Harrison[b*]

[a]Institute of Aircraft Design, University of Stuttgart, Germany

[b]School of Engineering, University of Glasgow, UK

* Corresponding author: P. Harrison, R509 Level 5, Systems Power and Energy, James Watt Building South, Glasgow G12 8QQ Tel.: +44 14 13 30 43 18. E-mail address: Philip.Harrison@glasgow.ac.uk

Abstract

An investigation has been conducted to evaluate the performance of normalisation methods for the uniaxial bias extension test. The predictions of two published theories for rate-independent behaviour are examined and a third heuristic method is proposed. Using hypothetical test data, the predictions of the two rate-independent theories are shown to be equivalent for specimen dimensions of high aspect ratio; in this case the predictions can be well-represented using the simple heuristic formula. The predictions diverge for specimens of low aspect ratio, when specimens are sheared to very high shear angles. In order to examine the significance of this divergence on real data, results from tests on several different engineering fabrics are normalised. Differences in the predictions of the normalisation methods are observed and the question of the significance of these differences is discussed. The paper also examines the applicability of rate-independent theory for normalising rate-dependent materials.

Keywords

A. Fabrics/textiles; B. Mechanical properties; C. Analytical modelling; D. Mechanical testing; E. Forming,

1. Introduction

Manufacture of advanced composites through automated press-forming is a viable technique for low-cost manufacture of complex 3-D components, promising large reductions in labour costs when compared with equivalent hand-layup processing methods. Forming of engineering fabrics coupled with liquid moulding technologies is a well-established route in the production of complex 3-d

advanced composite components [1]. The development of Computer Aided Engineering tools to support forming processes for advanced composites and engineering fabrics is a necessary requirement for widespread uptake of automated production technologies. This requirement has motivated a large amount of research, across both academia and industry, to develop constitutive models to describe the large deformation mechanics of engineering fabrics, suitable for implementation in finite element software [2-8]. Depending on the complexity of the constitutive model, various characterisation tests are required to determine the relevant constitutive model parameters.

It is well known that the forming behaviour of biaxial engineering fabrics is facilitated by their ability to undergo large shear strains, while strains along their fibre directions remain relatively low. The 'formability' of engineering fabrics is determined in large part by the shear-compliance of the fabric [9]. The importance of the shear behaviour means that various tests have been devised to characterise fabric shear compliance, the most commonly used methods are the Picture Frame and the Uniaxial Bias Extension (UBE) tests [10, 11]. Problems associated with these two test methods are well-documented: The Picture Frame test produces almost homogenous kinematics throughout the test specimen but is extremely sensitive to specimen misalignment issues [11]. In contrast, the UBE test is relatively insensitive to specimen misalignment but induces non-homogenous kinematics across the test specimen making it more difficult to interpret results and the test is also susceptible to intra-ply slip as the fabric reaches relatively high shear angles [12]. This slip limits the maximum shear angle that can be explored using the UBE test. These issues have motivated the introduction of variations on these shear test methods in recent years [13, 14]. Nevertheless, the simplicity and familiarity of the Picture Frame and UBE tests means they currently remain the preferred shear test methods for many researchers working in the field of composites forming [15] and are also often used to check the measurements produced using alternative new shear test techniques [16]. The standard Picture Frame and UBE tests therefore remain important methods for the characterisation of fabric forming mechanics. The main goal of these tests is to produce a specimen size-independent measure of the shear resistance of the fabric, for a Picture Frame test this is easily found and is usually expressed as the shear force per unit length, e.g. from [17];

$$F_{sh}(\theta) = F_{pf}/2L_{pf}cos\left(\frac{\pi}{4} - \frac{\theta}{2}\right) \quad \text{Eq 1}$$

where F_{sh} is the normalised shear force per unit length, F_{pf} is the axial force measured during the picture frame tests, L_{pf} is the side length of the picture frame rig and θ is the shear angle of the specimen in the picture frame rig. Note that in some instances, researchers prefer to express the shear resistance as the torque, though this is can be easily related back to the F_{sh} (see, for example, [18]).

This paper focuses on the UBE test, more specifically on the normalisation methods that have been proposed to interpret data from this test for engineering fabrics, i.e. to find F_{sh} from the axial force, F_{be}, measured in the UBE test. The theory depends, not just on kinematic assumptions but also on the type of material response exhibited by the specimen. In the literature, two theories have been independently presented to normalise rate-independent fabrics; both theories assume that fabric shear compliance is purely a function of shear angle (or shear strain) and use power-based analyses to determine the underlying shear force from the UBE axial force, the theories can be found in [19, 20] and [10, 18, 21]. The two derivations are different and, as will be shown in this paper, the final normalisation equations are not the same; both equations require numerical iteration in order to extract the final shear force curve from the UBE axial force data. The aim of this investigation is to determine whether the two normalisation methods produce identical predictions, and if not, whether any differences are significant, under what conditions potential differences are likely to occur and if possible, which theory provides the more plausible results. The paper also examines the applicability of rate-independent theory for normalising rate-dependent materials (i.e. prepregs and thermoplastics above their melt temperature).

The structure of the remainder of this paper is as follows. The underlying assumptions of both rate-independent theories are first outlined and the main equations are provided. Theoretical evaluation of the theories is conducted using hypothetical shear force versus shear angle data. Next, both methods are used to normalise real data produced from three different classes of 'dry' (rate-independent) engineering fabric. A comparison of the normalised predictions is drawn and the results are discussed. A final investigation is conducted using data from a 'wet' (viscous or rate-dependent) textile to examine just how important the underlying assumptions of the normalisation theories are in determining the form of the resulting normalised data. The paper concludes with a short discussion of the main findings of the investigation.

2. Normalisation Theory for Rate Independent Fabrics

In this section the main assumptions and the normalisation equations resulting from these assumptions are provided.

2.1. Assumptions Regarding Sample Kinematics

The kinematics of the UBE test have been analysed in detail using various methods including manual [19] and automated image analysis [20] and also using digital image correlation techniques [22]. For the purposes of normalisation, the kinematics across the test specimen are often described using three distinct regions; A, B and C. Figure 1 shows these regions in a UBE test sample with an aspect ratio of 2; the test can also be conducted using test specimens of higher aspect ratio.

[Figure 1]

If the shear angle in region A is denoted by θ, then the shear angle in region B can be approximated as $\theta/2$, while Region C ideally remains in an un-deformed state throughout the test. Experimental measurements indicate this assumption is valid at low shear angles, but becomes less so as the shear angle increases. The range of validity depends very much on the fabric in question. The presence of in-plane bending stiffness can mean the transition from one region to another occurs over a finite transition distance [23], rather than as an abrupt change as depicted in Figure 1b and as the shear angle in region A increases, intra-ply slip becomes more important leading to, for example, deformation in Region C. Nevertheless, the three-region idealisation is useful in creating appropriate normalisation theory.

2.2. Assumptions Regarding Material Behaviour

Rate-independent normalisation theories assume that the fabric's shear resistance is purely a function of shear angle. Both theories considered in this investigation ignore the effects of shear tension coupling (where the shear resistance of biaxial woven engineering fabrics increases with increasing tensile stress along the fibre directions). The latter has been both measured [10, 24] and predicted [25, 26] in several investigations on woven fabrics; the effect has been found to be significant resulting in shear stiffness increases of several 100 per cent. Including this behaviour in the normalisation method is possible [27], though requires information regarding the tensile stress across the test specimen [28]. Given that the latter is difficult to obtain and also that the shear-

tension coupling is probably not active in some dry engineering fabrics, such as Non-Crimp Fabrics (NCFs), the two proposed 'uncoupled' theories discussed in this paper remain relevant. Such uncoupled theory and can be regarded as the foundation upon which more comprehensive theories can be built, e.g. [27]

2.3. Final Normalisation Equations

Using the assumptions for sample kinematics and material behaviour, two different theories have been proposed resulting in equations that can be employed to extract the normalised shear force per unit length from the measured UBE axial test force measured using the test machine. Both theories follow a stress power-based analysis, the final normalisation equation from the first theory can be presented as:

$$F_{sh}(\theta) = \frac{F_{be}(\theta)}{\sqrt{2}\cdot W}\cdot\frac{(\lambda-1)}{(2\lambda-3)}\cdot\frac{1}{cos(\pi/4-\theta/2)} - \frac{F_{sh}(\theta/2)}{(2\lambda-3)}\cdot\frac{cos(\pi/4-\theta/4)}{cos(\pi/4-\theta/2)}\cdot\frac{cos(\theta)}{cos(\theta/2)}\cdot\frac{[1+cos(\theta/2)-sin(\theta/2)]}{[1+cos(\theta)-sin(\theta)]} \quad \text{Eq 2}$$

here F_{sh} is the normalised shear force per unit length, F_{be} is the axial force measured in the UBE test, W is the width of the test specimen and λ is the aspect ratio of the sample ($\lambda = H/W$) where H is the height of the specimen (see Figure 1). This theory is referred to as 'Method 1: (Rate-Independent, 2007)' for the remainder of the paper, indicating a fundamental assumption of the theory and the year of publication. The reader is referred to [20] for a full description of the theory behind this equation and to Appendix 1 for a description of the steps required to express the relevant equations in this final form.

The second theory also follows a power analysis [10, 18, 21] and for the remainder of the paper is referred to as 'Method 2: (Rate-Independent, 2008)'. The reader is referred to [21] for details on the derivation of the final normalisation equation,

$$F_{sh}(\theta) = \frac{1}{(2H-3W)cos\theta}\left\{\left(\frac{H}{W}-1\right)\cdot F_{be}\cdot[cos(\theta/2)-sin(\theta/2)] - W\cdot F_{sh}(\theta/2)\cdot cos(\theta/2)\right\} \quad \text{Eq 3}$$

Note that both Eqs 2 and 3 have a similar form, i.e.

$$F_{sh}(\theta) = P(\theta,W,H)\cdot F_{be} - Q(\theta,W,H)\cdot F_{sh}(\theta/2) \quad \text{Eq 4}$$

where P and Q are simply functions of the shear angle and the aspect ratio of the test specimen. Because $F_{sh}(\theta)$ depends on its own value at $\theta/2$, i.e. $F_{sh}(\theta/2)$, iteration is required to find $F_{sh}(\theta)$. Various iterative algorithms can be implemented to solve these equations, though this introduces the possibility of error due to the iterative process. In order to evaluate the performance of these

equations without this potential error, Eqs 2 and 3 can be rearranged to make F_{be} the subject of the equations. Thus, from Eq 2,

$$F_{be}(\theta) =$$

$$\frac{\sqrt{2}\cdot W}{(\lambda-1)}\cdot\left\{F_{sh}(\theta)\cdot(2\lambda-3)\cdot cos\left(\frac{\pi}{4}-\frac{\theta}{2}\right)+F_{sh}(\theta/2)\cdot cos\left(\frac{\pi}{4}-\frac{\theta}{4}\right)\cdot\frac{cos(\theta)}{cos(\theta/2)}\cdot\frac{[1+cos(\theta/2)-sin(\theta/2)]}{[1+cos(\theta)-sin(\theta)]}\right\} \quad \text{Eq 5}$$

and from Eq 3, find

$$F_{be}=\frac{F_{sh}(\theta)\cdot(2H-3W)cos(\theta)}{(H/W-1)\cdot[cos(\theta/2)-sin(\theta/2)]}+F_{sh}(\theta/2)\cdot\frac{W\cdot cos(\theta/2)}{(H/W-1)\cdot[cos(\theta/2)-sin(\theta/2)]} \quad \text{Eq 6}$$

If the shear force per unit length is known 'a priori', then predictions for the UBE axial test force can be produced by each method and examined without any un-certainty due to use of iterative solution algorithms required to solve Eqs 2 and 3. Note that for real specimens, ideal trellis shear kinematics can occur up to shear angles of anywhere between 10 and 55 degrees (e.g. see Section 4) depending on the material being tested, before other deformation mechanisms, such as intra-ply slip begin to dominate e.g. [29]. However, the assumption of ideal kinematics used in deriving both Eqs 2 and 3 is valid for any shear angle (up to 90 degrees). As a result, examination of the predictions of these theories can be conducted to very high shear angles and still remain valid, i.e. predictions at very high shear angles are still consistent with the underlying assumptions used in the theory. This is useful when aiming to evaluate the predictions of these theories.

3. Evaluation of Normalisation Theories

In this section three different hypothetical shear force versus shear angle behaviours are postulated and fed into Eqs 5 and 6. The aim is to examine first of all whether the predictions of Methods 1: (Rate-Independent, 2007) and 2: (Rate-Independent, 2008) are the same and, if not, to evaluate the reasonableness of the respective predictions.

3.1. Evaluation of UBE Force Prediction using known Shear Force Behaviour

Three shear force (per unit length) versus shear angle behaviours are postulated in Eqs 7-9. Different materials are known to produce different forms for their shear force versus shear angle curves. Consequently, different behaviours are used in order to examine the effect of the shape of the underlying shear force versus shear angle curve on the resulting UBE axial force predictions.

$$F_{sh}=10\cdot\theta^{0.2}+10^{-9}\cdot\theta^{6} \quad \text{Eq 7}$$

$$F_{sh}=\theta \quad \text{Eq 8}$$

$$F_{sh} = \theta^{0.01} \quad \text{Eq 9}$$

Eq 7 provides a reasonably typical form for shear force versus shear angle curves observed during actual experimental testing, with a low initial force followed by a steep rise as the material approaches its locking angle. Eqs 8 and 9 are also included to examine the effect of deviations from this typical behaviour. Note however, that unlike the shear force curves expected for real materials, these hypothetical curves do not tend to infinity as the shear angle approaches 90°. Thus, at some shear angle these hypothetical curves will diverge away from likely 'realistic' material behaviour. From the perspective of testing the predictions of the two normalisation theories, the lack of realism here is irrelevant. Indeed, by tending towards a finite value, the forms of the shear force curves are beneficial in examining the predictions of the normalisation theories at high shear angles.

Choosing $W = \sqrt{2}$m in Eqs 4 and 5 means that the side length of Region A, L = 1m (see Figure 1). This allows the predicted UBE axial force predictions to be conveniently compared with the input shear force (per unit length) in the same graphs. Two values for the aspect ratio of the test specimen, λ=1000 and λ=2, are used to explore the effect of aspect ratio on the predictions. Feeding the known shear force functions (Eqs 7 to 9) into Eqs 5 and 6 and using these specimen dimensions produces the following results, see Figure 2.

[Figure 2]

Figure 2 shows that the UBE axial force predictions from Method 1: (Rate-Independent, 2007) and 2: (Rate-Independent, 2008) are almost identical for a test sample aspect ratio, λ=1000 (the UBE axial force curves predicted by the two methods are almost exactly superposed in Figures 2a, 2c & 2e). The fact that both methods produce almost identical results suggests both provide correct predictions for high aspect ratio samples, at least up to shear angles of 85°. Note also that for very large values of λ the second term on the right hand side of both Eqs 4 and 5 becomes negligible, and both equations can be approximated with Eq 10

$$F_{simple} = 2\sqrt{2}WF_{sh}cos(\pi/4 - \theta/2) \quad \text{Eq 10}$$

where F_{simple} represents the UBE axial force predicted using this relatively simple equation (again the UBE axial force curves predicted using Eq 5, 6 & 10 are almost exactly superposed in Figures 2a, 2c and 2e). This equation has also been found to provide reasonable predictions for smaller

values of λ and suggests a potentially much faster and simpler method for approximate normalisation of rate-independent data from UBE tests, referred to here as Method 3: (Approximation).

The situation changes when λ=2; an aspect ratio more relevant to actual UBE testing. Here the predictions of Methods 1: (Rate-Independent, 2007) and 2: (Rate-Independent, 2008) diverge when the shear angle grows larger than about 40°. The divergence increases moving from plots produced using Eqs 7 to 9. The UBE axial force predictions of Method 2: (Rate-Independent, 2008) tend towards infinity as the shear angle tends towards 90°. In contrast, the predictions of Method 1: (Rate-Independent, 2007) stay close to the underlying shear force input curve. Detailed examination of the contributions from Regions A and B to the total UBE axial force, show that both methods predict exactly the same force contribution from Region A. The difference between the two theories lies entirely in their predicted contributions from Region B. To illustrate, the relative contribution from Region A and Region B, i.e. (Force contribution due to shearing of Region B)/ (Force contribution due to shearing of Region A) for both sample aspect ratios, λ=1000 and λ=2, is plotted in Figure 3. Note the large difference in the vertical scale of the two plots. The forms of the 'contribution ratio' versus shear angle curves are independent of the specimen aspect ratio for both Methods 1: (Rate-Independent, 2007) and 2: (Rate-Independent, 2008).

[Figure 3]

Referring to Figure 3, both Methods 1: (Rate-Independent, 2007) and 2: (Rate-Independent, 2008) predict the same contribution ratio for small shear angles, for both λ=1000 and λ=2. The difference between the predicted force contributions from Region B grows as the shear angle increases. Since both methods predict exactly the same contribution from Region A, the difference in the force contribution from Region B results in different 'contribution ratios'. For samples with a high aspect ratio, i.e. with λ=1000 (see Figure 3a), the relative contribution from Region B is very small, consequently the influence of Region B on the total UBE axial force curves is negligible and both Methods 1: (Rate-Independent, 2007) and 2: (Rate-Independent, 2008) predict almost the same result (see Figures 2a, 2,c and 2e). In contrast, for samples with a low aspect ratio, i.e. with λ =2 (see Figure 3b), the relative contribution from Region B is significant, consequently the influence of Region B on the total UBE axial force curves is noticeable (see Figures 2b, 2d and 2f).

Method 2: (Rate-Independent, 2008) predicts that the relative contribution from Region B tends towards infinity as the shear angle approaches 90° (reflected in the sharply increasing ratio of Contribution B/Contribution A in Figure 3), this is not physically reasonable and suggests a problem with Method 2: (Rate-Independent, 2008) that leads to error at large shear angles. The difference between the predictions of the two methods only becomes noticeable at high shear angles (> 30°) and the size of the difference strongly depends on the shape of the shear force input curve; it is smaller for input shear force curves showing an exponential increase, e.g. Eq 7.

Given that Methods 1: (Rate-Independent, 2007) and 2: (Rate-Independent, 2008) arise from different derivations and their predictions for large values of λ are almost exactly the same, this provides reasonable confidence (but not absolute proof) that both theories are at least approximately correct when analysing this particular scenario, i.e. the predictions for Region A by both theories is most likely correct. When analysing small values of λ, the unrealistic prediction for the contribution to the force from Region B, produced by Method 2: (Rate-Independent, 2008) suggests a problem with this theory. Clearly, the problem with Method 2: (Rate-Independent, 2008) is not a proof of the accuracy for Method 1: (Rate-Independent, 2007), although the consistency and reasonableness of the predictions from the latter are indicative that its predictions are most likely correct. It can therefore be concluded that Method 1: (Rate-Independent, 2007) probably provides a more accurate result (within the assumptions used to formulate the two normalisation theories) and that the differences between the predictions of Methods 1:(Rate-Independent, 2007) and 2: (Rate-Independent, 2008) are more noticeable when: (i) the test specimen aspect ratio is low and (ii) the test data reach high shear angles. The shape of the input curve also plays a role; the difference between the predictions of the two theories increases when: (iii) the shear force versus shear angle data increases approximately linearly or (iv) the shear force versus shear angle data has an initial sharp increase at low shear angles followed by a plateauing or shallow increase at moderate angles, followed by a sharply increasing force at higher shear angles. Condition (iv) is expected to create greater differences than condition (iii), (due to the increased significance of the force contribution of Region B relative to Region A throughout the course of a test).

Turning briefly to the predictions of Method 3: (Approximation), these lay further from those of Method 1: (Rate-Independent, 2007) than do those of Method 2: (Rate-Independent, 2008) in Figure 2b. However, in Figures 2d and 2e, the opposite is true. In all three cases Method 3:

(Approximation) is very close to Method 1: (Rate-Independent, 2007) at angles less than 40° and reasonably close at higher shear angles. In the next section, the question of whether these differences are observable when normalising actual test data, is examined.

4. Normalisation of Experimental Results

UBE axial force results obtained by tests conducted using four different fabrics are presented. The data are normalised using Methods 1: (Rate-Independent, 2007), 2: (Rate-Independent, 2008) and 3: (Approximation) in order to determine whether the difference in predictions discussed in Section 3.1 has any noticeable effect on the final normalised results. To this end, tests on three dry engineering fabrics, using three different specimen aspect ratios, have been conducted and the data has been normalised. Finally, normalisation of UBE tests conducted on a wet fabric (containing a liquid matrix phase), first using the 3 dry fabric normalisation theories (Methods 1 to 3) and second using the viscous fabric normalisation theory presented previously [16] i.e. Method 4: (Rate-dependent, 2004) is performed (the name indicates the rate-dependency (Newtonian assumption used in the theory) and the year of publication of this theory). The aim of the final comparison is to understand the effect of the underlying assumptions on the form of the resulting normalised data, i.e. does it matter which theory is used?

4.1. Materials and Test Set-up

Three different classes of engineering fabric were chosen for the investigation of dry fabrics using three different specimen dimensions, images are provided in Table 1. The first material is a Twintex 22 plain weave co-mingled fabric from FiberGlass Industries consisting of glass and polypropylene (PP) fibres, with an areal density of about 750 g/m^2 and a tow width of 4 mm. Specimens were cut with unclamped dimensions of H=225 mm and W=75 mm (λ=3).

The second material is a balanced biaxial non-crimp fabric consisting of T700 carbon fibre and a standard PE tricot stitch. The areal density is about 400 g/m^2. Specimens were cut with unclamped dimensions of H=200 and W=75mm (λ=2.67).

The third material is a predominantly unidirectional carbon fabric, the integrity of the fabric is provided by a thin glass roving orthogonal to the main fibre direction. The two constituents are held together using a polyethylene (PE) tricot stitch. The areal density is 333 g/m^2. Specimens were cut with unclamped dimensions of H=100 mm and W=50 mm (λ=2).

Tests on dry fabrics were conducted at room temperature using a novel built test machine (Tension-Shear-Compression tester) fitted with a 100 N load cell. Shear angles were measured using automated optical analysis. After each millimetre of movement a picture was taken and the area of constant shearing (Region A) was used to automatically analyse (24 angles measured per picture) a mean shear angle [15].

For the final comparison using a viscous textile composite, a Twintex 2x2 twill weave pre-consolidated glass-PP composite with an areal density of 745 gm-2, (fibre volume fraction = 0.35, thickness = 0.54mm) and unclamped specimen dimensions of H=200 mm and W=100 mm (λ =2) was used [17]. Tests were conducted at 200^{o}C at a constant crosshead displacement rate of 400mm/min, using a Hounsfield universal test machine fitted with a 1000 N load cell. Shear angles were measured by manual image analysis of video data. Data were averaged from 3 tests.

Fabric kinematics measured in each test are illustrated in Figure 4. The different fabric and sample size used in each test means that intra-ply slip occurs to a greater or lesser extent in each of the cases. Larger specimen sizes are expected to lead to greater specimen integrity. Normalised shear force data are shown in Figure 5. Data measured at shear angles at which intra-ply slip was significant is highlighted using the shaded areas in Figure 5. It should be noted that testing of non-crimp and unidirectional fabrics in the UBE test is debatable and not yet standard practice, e.g. [30]; the test is more commonly reserved for biaxial woven fabrics, the latter are often assumed to undergo more 'ideal' trellis shear kinematics when pulled in their bias direction. The extent of the intra-ply slip as a proportion of the entire shear force versus shear angle curve is a measure of the test specimen 'integrity'. The maximum shear angle achieved by the specimen is an indication of its 'formability'. For example, Figure 5 indicates the UD fabric specimen has a very low integrity and high formability while the plain weave fabric specimen has high integrity but relatively low formability. Given that the normalisation theories take no account of slip mechanisms, the accuracy of normalising data in this region is arguable. For example, if intra-ply slip mechanisms act in series with sample extension due to trellis shear, then the error is likely to be small. This can be compared with the situation where the modulus of a stiff sample, e.g. steel, is measured in a tensile test using a relatively compliant test machine. If a strain gauge is used to determine the strain in the steel tensile specimen, then the error due to the compliance of the test machine is eliminated and the measurement of the modulus is still accurate. Measuring the shear angle across a fabric specimen

using image analysis is equivalent to using a strain gauge. If however the fabric slip mechanisms act in parallel with the trellis shear extension of the fabric (i.e. their action doesn't increase sample length) then the error could be significant. This point requires further investigation and is deferred to future work.

[Table 1]

[Figure 4]

[Figure 5]

Following the analysis of Section 3.1, it is assumed that Method 1: (Rate-Independent, 2007), predicts the correct result. Thus, to quantify the error in Methods 2: (Rate-Independent, 2008) and 3: (Approximation), the relative difference of their predictions with those of Method 1: (Rate-Independent, 2007) can be expressed in terms of the shear force at a given shear angle, or the shear angle at a given shear force. These relative errors are calculated at the maxima of each data set plotted in Figure 5.

Experiment 1: Co-mingled plain weave fabric

The first experiment used a plain weave co-mingled fabric and a high specimen aspect ratio of λ=3. Intra-ply slip became significant at around 42^{o}. The shear force curve increased exponentially at a relatively low shear angle. According to the analysis in Section 3.1, these conditions favour only a small difference between the predictions of Methods 1: (Rate-Independent, 2007) and 2: (Rate-Independent, 2008). The error in Method 2: (Rate-Independent, 2008) at the maximum force is negligible (about 0.5% lower force and 1% higher shear angle). The error in the prediction of Method 3: (Approximation) is more notable (23% lower force and 7% higher shear angle).

Experiment 2: NCF fabric

The second experiment used a NCF fabric and a medium specimen aspect ratio of λ=2.67. Intra-ply slip became significant at around 52^{o}. The shear force curve increased exponentially at a high angle. According to the analysis in Section 3.1, the higher shear angles achieved by the NCF favour a larger difference between the predictions of Methods 1: (Rate-Independent, 2007) and 2: (Rate-Independent, 2008) than in Experiment 1. Indeed, the error in the prediction of Method 2: (Rate-Independent, 2008) at the maximum force is slightly higher than for experiment 1 but is still very small (about 4% lower force and 0.2% higher shear angle). The error in the prediction of Method 3: (Approximation) is again more notable (28% lower force and 1.7% higher shear angle).

Experiment 3: UD sewn fabric

The third experiment used a UD sewn fabric and a low specimen aspect ratio of λ=2. Intra-ply slip became significant at just 10° partly due to the nature of the fabric architecture and party due to the small specimen size. The shear force curve increased approximately linearly with shear angle. According to the analysis in Section 3.1, the higher shear angles achieved by the UD fabric coupled with the more linear shear force curve, favours a larger difference between the predictions of Methods 1: (Rate-Independent, 2007) and 2: (Rate-Independent, 2008). As expected, the error in the prediction of Method 2: (Rate-Independent, 2008) at the maximum force is now more noticeable (about 21% difference in force and 6.5% difference in shear angle) while the error in the prediction of Methods 3: (Approximation) is larger still (35% lower force and 14% higher shear angle). Note that intra-ply slip is a very significant mode of deformation for this material.

Experiment 4: Co-mingled Twill weave fabric at 200°C

The fourth experiment used a twill weave pre-consolidated composite sheet and a low specimen aspect ratio of λ=2. Tests were conducted at 200°C in order to melt the PP phase of the composite, creating a 'wet' textile with a strain rate-dependent response [19, 31]. Intra-ply slip became significant at about 45°. In this example, the rate dependence of the material means that it no longer conforms to the strain rate-independent assumptions used in formulating the theories of Methods 1: (Rate-Independent, 2007) or 2: (Rate-Independent, 2008). The 'viscous' normalisation theory presented in [19] is also applied, i.e. Method 4: (Rate-dependent, 2004); the latter requires no iterative method to retrieve the shear force but does involve a Newtonian approximation which undoubtedly introduces some error. Referring to Figure 5d, the most notable aspect of the rate-independent normalisation predictions is the negative gradient observed between shear angles of about 20° and 40°. This negative gradient is not predicted by Method 4: (Rate-dependent, 2004), the viscous normalisation theory. (The reason for this is that in the viscous theory, Region A dominates the samples response, not just because of the relatively high shear strain in this region compared to that in Region B, but also due to the higher shear strain rate in Region A. This effectively reduces the 'softening effect' associated with the predictions of the rate-independent theories). Introducing shear force versus shear angle curves with negative gradients into constitutive models could potentially cause numerical issues in finite element simulations. Consequently, use of rate-independent theory to normalise results from rate-dependent materials

may, in certain cases, produce problematic results. Having said this, the use of a Newtonian approximation in the viscous theory is not ideal and a more accurate rate-dependent normalisation theory is desirable, though this undertaking is deferred to future work. Divergence in the predictions of Method 3: (Approximation) and Method 1: (Rate-Independent, 2007) are large for this case; 45% lower force and 11% higher shear angle compared to Method 1: (Rate-Independent, 2007).

5. Conclusions

The investigation has compared two different normalisation theories developed previously for 'dry' strain rate-independent engineering fabrics and also suggested a third much simpler normalisation technique, Method 3: (Approximation). Method 1: (Rate-Independent, 2007), 2: (Rate-Independent, 2008) and 3: (Approximation) provide almost exactly the same predictions for specimens of very high aspect ratios. For specimens of lower aspect ratio (with λ around 2), the predictions diverge at high shear angles, in this case Method 2: (Rate-Independent, 2008) overestimates the force contribution from Region B, introducing some degree of error. The size of this error depends on the form of the shear force versus shear angle data to be normalised. Comparison of normalised results produced using real experimental data suggests this error is negligible for typical dry woven fabrics and NCFs. Method 3: (Approximation) produces less accurate results with a maximum error of 7% at the highest shear angles for dry woven fabrics and NCFs, though this error is much lower at lower shear angles. Normalisation of UD fabric shows larger deviations between the 3 methods, though use of these normalisation theories for this type of fabric is questionable due to the large degree of intra-ply slip present during testing. The final example, which involved normalisation of a strain rate-dependent fabric, revealed a relatively large difference in predictions when employing the strain rate dependent; Method 4: (Rate-dependent, 2004) and strain rate independent methods; Method 1: (Rate-Independent, 2007) and 2: (Rate-Independent, 2008). The simplest method, Method 3: (Approximation), also produced very large errors in this example.

This investigation raises the question of how accurate the normalised shear force versus shear angle data need to be. For the dry fabric data, Methods 1 to 3 all capture the general form of the data fairly well, to within just a few per cent error. All of the methods clearly distinguish the different shear force versus shear angle behaviours produced by the plain weave and the NCF. Such

large differences are expected to produce significant changes in the predictions of complex forming simulations, such as shear angle and wrinkling [2, 31, 32]. In contrast, differences of less than 1 % between Methods 1: (Rate-Independent, 2007) and 2: (Rate-Independent, 2008) or even less than 7% between Methods 1: (Rate-Independent, 2007) and 3: (Approximation), produced when normalising the same test data using different normalisation methods, is unlikely to produce much notable difference in finite element simulations. For this reason, use of Method 3: (Approximation) might be deemed acceptable for most practical purposes, motivated by the ease and simplicity of its application. The main value and justification for developing more complex but more accurate normalisation theory is therefore, not in finding, for example, a 0.5% or 1% improvement in the accuracy of the final normalised data, but rather in providing a means to determine the 'correct' result by which other simpler and faster normalisation methods can be assessed. Following this line of reasoning, further effort in enhancing existing theory might be justified. For example, introducing assumptions to include the effects of a shear-tension coupling for dry rate-independent fabrics could result in further changes in the form of the final normalised data and could also help account for possible size-effects when testing samples of different absolute size (due to the generation of higher tensile forces). Alternatively, the effect of including non-Newtonian behaviour rather than using a Newtonian assumption in the normalisation theory for wet rate-dependent fabrics could help in determining if the negative gradients observed in the normalised data in this investigation are real or merely artefacts produced by the normalisation method [33]. Once the 'correct' result is known, then any error associated with use of simpler normalisation methods can be properly stated and consideration of the likely influence of such error on, for example, forming simulation predictions, can be properly assessed.

Acknowledgment

The authors would like to thank the Department of Science, Research and Art Baden Wurttemberg (AZ32-729.85-1/90) for supporting the work presented here.

Appendix: Derivation of Eq 1

Eq 2 is presented for the first time in this paper and is obtained following a few algebraic manipulations of the theory presented in [20]. These steps are provided here for clarity and to be understood, must be read together with Harrison et al. 2008; the reader is referred to the latter for definition of all terms. References to equations in [20] are indicated here using the format (H-*). For example, Eq (H-1) indicates Eq 1 in [20].

Starting from Eq (H-34) find,

$$k_2(\theta) = \frac{d_5}{(\lambda - 1)L_5 \cos\theta} \tag{A1}$$

Thus,

$$k_2\left(\frac{\theta}{2}\right) = \frac{d_5}{(\lambda - 1)L_5 \cos(\theta/2)} \tag{A2}$$

and

$$k_2\left(\frac{\theta}{2}\right) \Big/ k_2(\theta) = \frac{\cos\theta}{\cos(\theta/2)} \tag{A3}$$

Also, combining Eq (H-26) and (H-32), find,

$$\psi(\theta) = \frac{F_1(\theta) \cdot k_2(\theta)}{L_1} \tag{A4}$$

From Eq (H-1), note that,

$$N_s(\theta) = F_s(\theta) = \frac{F_1(\theta)}{2L_1 \cos\Phi} \tag{A5}$$

Thus, using Eq (H-2) find

$$F_1(\theta) = 2F_s(\theta)L_1 \cos\left(\frac{\pi}{4} - \frac{\theta}{2}\right) \tag{A6}$$

Substitute Eqs (A6) in (A4), to find,

$$\psi(\theta) = 2F_s(\theta)L_1 \cos\left(\frac{\pi}{4} - \frac{\theta}{2}\right) \cdot k_2(\theta) \tag{A7}$$

and note that,

$$\psi\left(\frac{\theta}{2}\right) = 2F_s\left(\frac{\theta}{2}\right)L_1 \cos\left(\frac{\pi}{4} - \frac{\theta}{4}\right) \cdot k_2\left(\frac{\theta}{2}\right) \tag{A8}$$

Referring to Fig 7 in [20], note that, $F_5 = F_{be}$ and $L_5 = W/\sqrt{2}$. Substitute these terms into Eq (H-31) and rearrange to make F_{be} the subject of the equation. Next, substitute in Eqs (A3), (A7) and (A8) to the result to find Eq 2 of the current paper.

Reference

[1] Vernet N, Ruiz E, Advani S, Alms JB, Aubert M, Barburski M, Barari B, Beraud JM, Berg DC, Correia N, Danzi M, Delavière T, Dickert M, Di Fratta C, Endruweit A, Ermanni P, Francucci G, Garcia JA, George A, Hahn C, Klunker F, Lomov SV, Long, A, Louis B, Maldonado J, Meier R, Michaud V, Perrin H, Pillai K, Rodriguez E, Trochu F, Verheyden S, Wietgrefe M, Xiong W, Zaremba S, Ziegmann G. Experimental Determination of the Permeability of Engineering Textiles: Benchmark II. Composites Part A: Applied Science and Manufacturing 2014;61:172-184

[2] De Luca P, Lefebure P, Pickett AK. Numerical and experimental investigation of some press forming parameters of two fibre reinforced thermoplastics: APC2-AS4 and PEI-CETEX. Composites Part A 1998;29:101–110.

[3] McEntee SP, O_Bradaigh CM. Large deformation finite element modelling of single-curvature composite sheet forming with tool contact. Composites Part A 1998;29 207–213.

[4] Boisse, P, Borr M, Buet K, Cherouat A. Finite element simulations of textile composite forming including the biaxial fabric behavior. Composites Part B: Engineering 1997;28(4):453–464.

[5] Yu WR, Harrison P, Long AC. Finite Element Forming Simulation for Non-crimp Fabrics Using a Non-orthogonal Constitutive Equation, Composites Part A 2005;36(8):1079–1093.

[6] Peng XQ, Cao J. A Continuum Mechanics Based Non-orthogonal Constitutive Model for Woven Composite Fabrics, Composites: Part A 2005;36:859–874.

[7] ten Thije RHW, Akkerman R, Huétink J. Large deformation simulation of anisotropic material using an updated Lagrangian finite element method. Computer Methods in Applied Mechanics and Engineering 2007; 196(33–34):3141–3150

[8] Zouari, Jean-Luc Daniel, Philippe Boisse, A woven reinforcement forming simulation method. Influence of the shear stiffness, Computers & Structures 2006;84(5-6):351-363

[9] Lomov SV, Barburski M, Stoilova TZ, Verpoest V, Akkerman R, Loendersloot R, R.H.W. ten Thije RHW. Carbon composites based on multiaxial multiply stitched preforms. Part 3: Biaxial tension, picture frame and compression tests of the preforms. Composites: Part A 2005;36:1188–1206

[10] Launay J, Hivet G, Duong AV, Boisse P. Experimental analysis of the influence of tensions on in plane shear behaviour of woven composite reinforcements. Compos Sci Technol 2008;68:506–515.

[11] Lebrun G, Bureau MN, Denault J. Evaluation of bias-extension and picture-frame test methods for the measurement of intraply shear properties of PP/glass commingled fabrics. Composite Structures 2003;61(4):341–352

[12] Wang J, Page JR, Paton R. Experimental investigation of the draping properties of reinforcement fabrics, Composites Science and Technology 1998;58:229-231

[13] Potluri P, Atkinson J. Automated manufacture of composites: handling, measurement of properties and lay-up simulations. Composites Part A: Applied Science and Manufacturing 2003;34 (6):493–501

[14] Milani AS, Nemes JA, Lebrun G, Bureau M. A Comparative Analysis of a Modified Picture Frame Test for Characterization of Woven Fabrics. Polymer Composites 2009;31(4):561-568

[15] Larberg Y, Åkermo M. In-plane deformation of multi-layered unidirectional thermoset prepreg – Modelling and experimental verification. Composites Part A: Applied Science and Manufacturing 2014;56:203-212

[16] Härtel F, Böhler P, Middendorf P. An integral mesoscopic material characterization approach, Key Engineering Materials 2014;611-612:280-291

[17] Harrison P, Clifford MJ, Long AC. Shear characterisation of viscous woven textile composites: a comparison between picture frame and bias extension experiments. Composites Science and Technology 2004;64(10-11):1453–1465

[18] Cao J, Akkerman R, Boisse P, Chen J, Cheng HS, de Graaf EF, Gorczyca JL, Harrison P, Hivet G, Launay J, Lee W, Liu L, Lomov SV, Long AC, de Luycker E, Morestin F, Padvoiskis J, Peng XQ, Sherwood J, Stoilova TZ, Tao XM, Verpoest I, Willems A, Wiggers J, Yu TX, Zhu B. Characterization of mechanical behavior of woven fabrics: Experimental methods and benchmark results. Composites: Part A 2008; 39:1037–1053

[19] Harrison P, Wiggers J, Long AC. Normalization of Shear Test Data for Rate Independent Compressible Fabrics, In: 10th International ESAFORM Conference on Materials Forming, 18–20th April, Zaragoza, Spain, 1011–1016.

[20] Harrison P, Wiggers J, Long AC. Normalization of Shear Test Data for Rate-independent Compressible Fabrics. Journal of Composite Materials 2008;42:2315-2344

[21] Hivet, G.; Duong, Ahn Vu, «A contribution to the analysis of the intrinsic shear behaviour of fabrics», Journal of Composite Materials 2011; 45 (6):695-717

[22] Lomov SV, Boisse P, Deluycker E, Morestin F, Vanclooster K, Vandepitte D, Verpoest I, Willems A. Full-field strain measurements in textile deformability studies. Composites Part A: Applied Science and Manufacturing 2008;39 (8):1232-1244

[23] Ferretti M, Madeo A, dell'Isola F, Boisse P. Modeling the onset of shear boundary layers in fibrous composite reinforcements by second-gradient theory. Z. Angew. Math. Phys. 2013

[24] Harrison P, Abdiwi F, Guo Z, Potluri P, Yu WR. Characterising the shear–tension coupling and wrinkling behaviour of woven engineering fabrics. Composites Part A: Applied Science and Manufacturing 2012;43(6):903-914

[25] Lomov SV, Verpoest I. Model of shear of woven fabric and parametric description of shear resistance of glass woven reinforcements. Composites Science and Technology 2006;66(7-8):919-933

[26] Lee W, Cao J, Badel P, Boisse P. Non-orthogonal constitutive model for woven composites incorporating tensile effect on shear behavior. J Mater Form 2008;1(Suppl.):891–894.

[27] Harrison P. Normalisation of biaxial bias extension test results considering shear tension coupling. Composites: Part A 2012;43:1546–1554

[28] Hivet, G.; Vidal-Sallé, E.; Boisse, P., «Analysis of the stress components in a textile composite reinforcement», Journal of Composite Materials 2013;, 47(3):269-285

[29] S. Gatouillat, A. Bareggi, E. Vidal-Sallé, P. Boisse, Meso modelling for composite preform shaping – Simulation of the loss of cohesion of the woven fibre network, Composites Part A: Applied Science and Manufacturing, Volume 54, November 2013, Pages 135-144

[30] Long Li, Yan Zhao, Ha-gia-nam Vuong, Yuan Chen, Jin Yang, Yuexin Duan, In-plane shear investigation of biaxial carbon Non-Crimp Fabrics with experimental tests and finite element modeling, Materials & Design, Available online 17 July 2014, ISSN 0261-3069, http://dx.doi.org/10.1016/j.matdes.2014.07.007.

[31] Wang P, Hamila N, Pineau P, Boisse P. Thermomechanical analysis of thermoplastic composite prepregs using bias-extension test. Journal of Thermoplastic Composite Materials 2014;27(5):679-698.

[32] Peng X, Rehman ZU. Textile composite double dome stamping simulation using a non-orthogonal constitutive model. Composites Science and Technology 2011;71:1075-1081

[33] Milani AS, Nemes JA, Abeyaratne RC, Holzapfel GA. A method for the approximation of non-uniform fiber misalignment in textile composites using picture frame test. Composites Part A: Applied Science and Manufacturing 2007;38(6):1493-1501

Figure 1. An idealised bias extension test sample with H/W = 2 (a) prior to deformation and (b) after deformation (adapted from [17]).

Figure 2. UBE and axial force predictions using Methods 1 to 3 for: (a) Eq 6 with λ =1000, (b) Eq 6 with λ =2 (c) Eq 7 with λ =1000, (d) Eq 7 with λ =2, (e) Eq 8 with λ =1000 and (f) Eq 8 with λ =2.

Figure 3. Ratio of the force contributions from Region B and Region A to the total UBE axial force for a sample aspect ratio of: (a) λ =1000 and (b) λ =2. The input equations used to create the curves are given in the legend.

Figure 4. Sample kinematics for the four different materials. Significant deviation (>5%) between ideal and measured kinematics occurs at about 42° for the plain weave, 52° for the NCF, 10° for the UD, and 45o for the Twill weave, the latter tested at 200°C.

Figure 5. Normalised shear force versus measured shear angle for: (a) plain weave, (b) NCF, (c) UD and (d) twill weave tested at 200°C. The shaded areas represent the shear angles at which intra-ply slip becomes significant

Figures

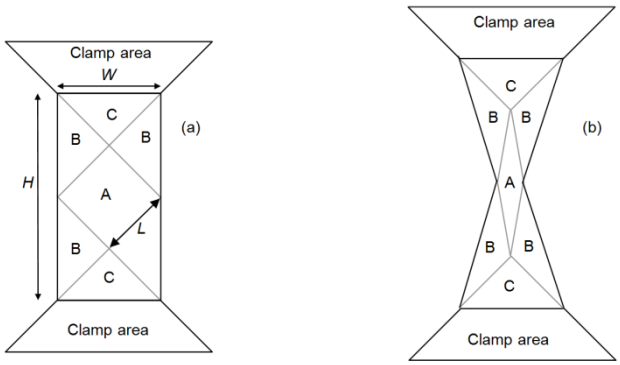

Figure 1. An idealised bias extension test sample with H/W = 2 (a) prior to deformation and (b) after deformation (adapted from [17]).

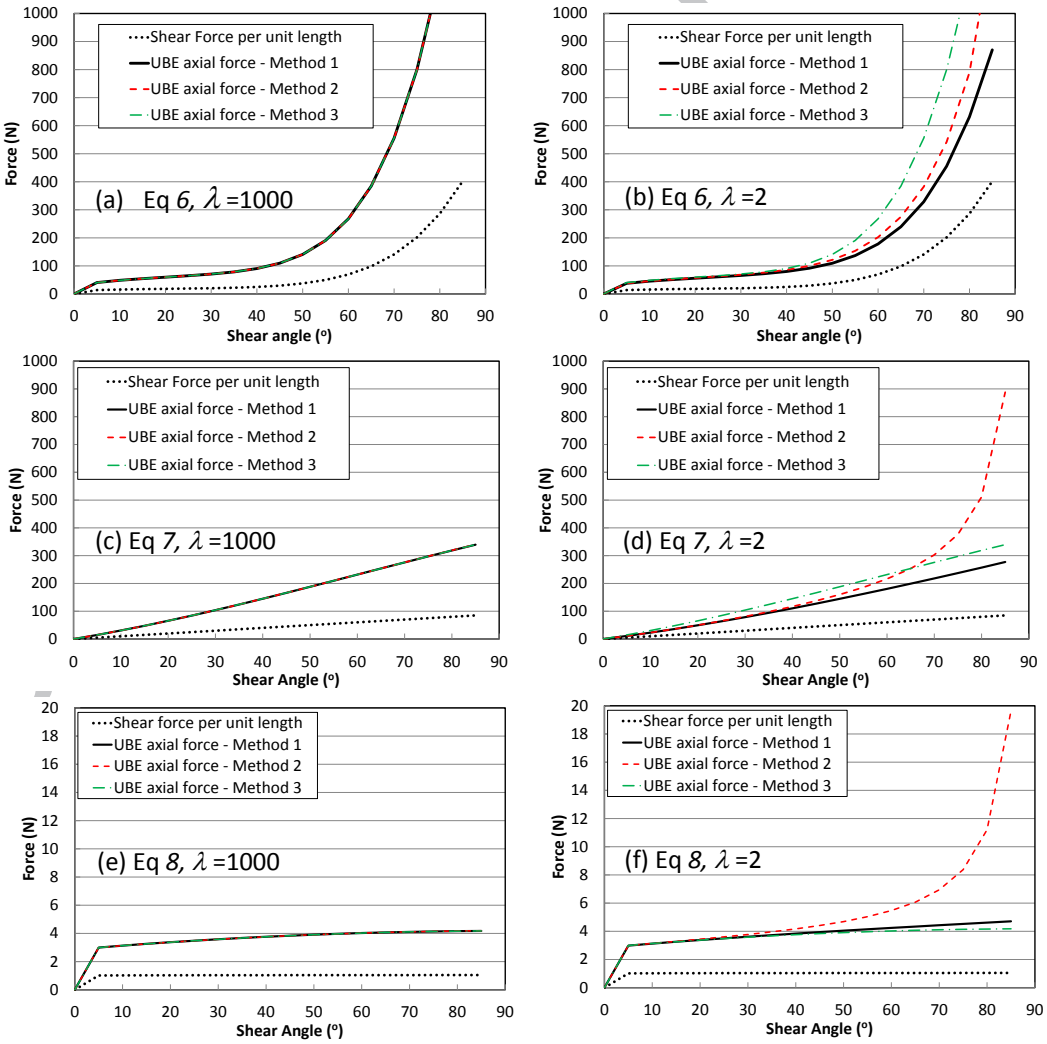

Figure 2. UBE and axial force predictions using Methods 1 to 3 for: (a) Eq 6 with λ =1000, (b) Eq 6 with λ =2 (c) Eq 7 with λ =1000, (d) Eq 7 with λ =2, (e) Eq 8 with λ =1000 and (f) Eq 8 with λ =2.

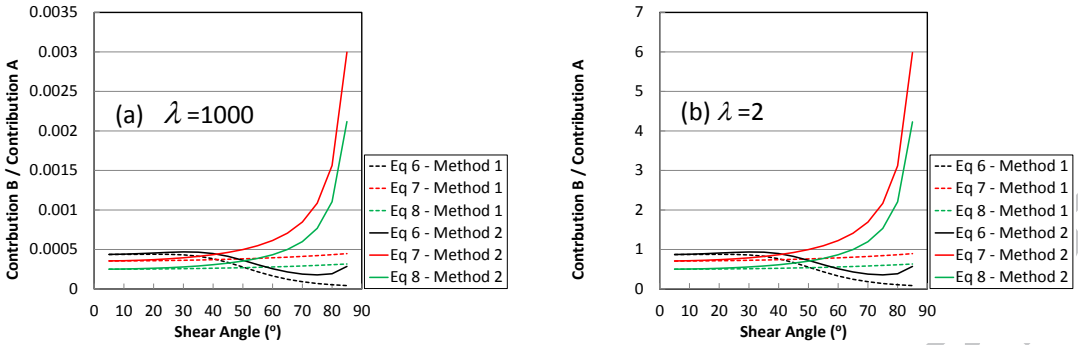

Figure 3. Ratio of the force contributions from Region B and Region A to the total UBE axial force for a sample aspect ratio of: (a) λ =1000 and (b) λ =2. The input equations used to create the curves are given in the legend.

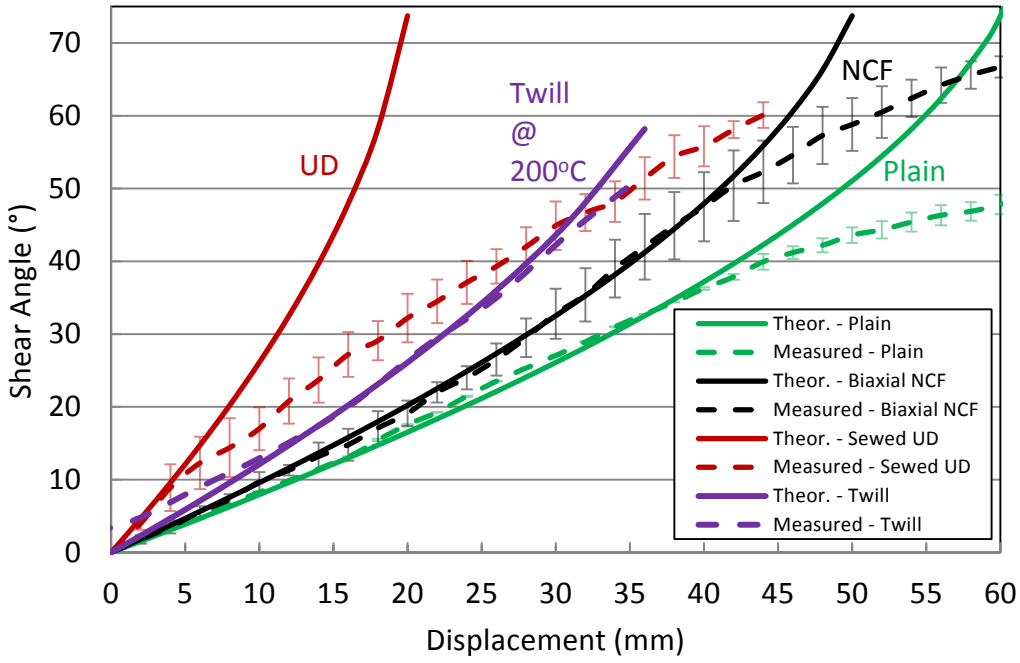

Figure 4. Sample kinematics for the four different materials. Significant deviation (>5%) between ideal and measured kinematics occurs at about 42° for the plain weave, 52° for the NCF, 10° for the UD, and 45° for the Twill weave, the latter tested at 200°C.

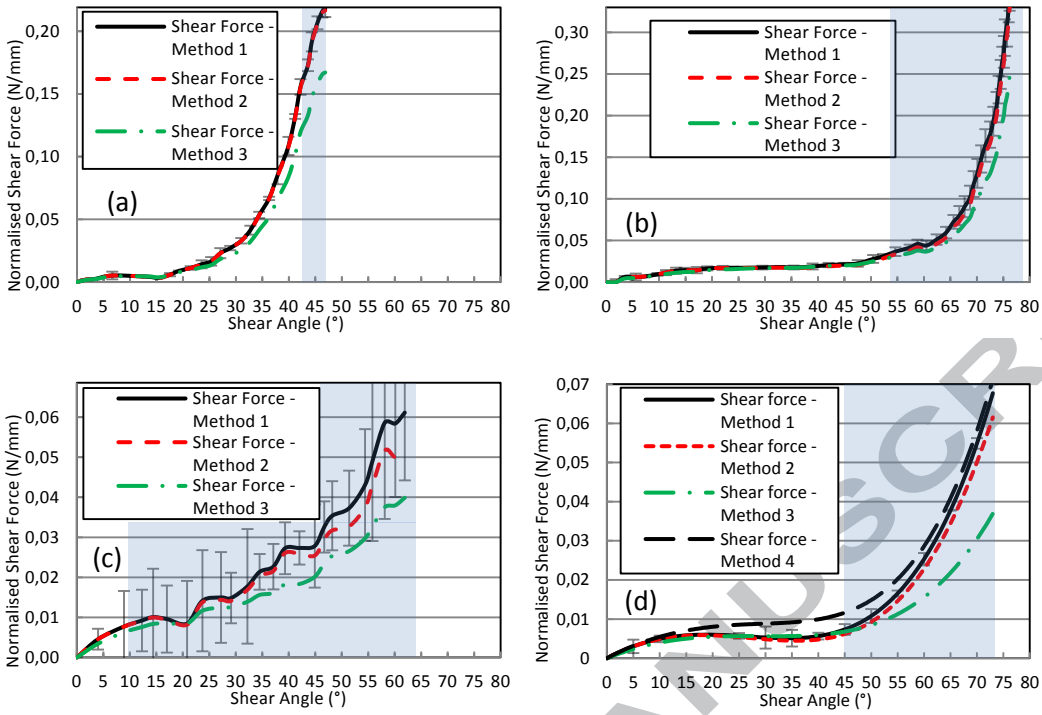

Figure 5. Normalised shear force versus measured shear angle for: (a) plain weave, (b) NCF, (c) UD and (d) twill weave tested at 200°C. The shaded areas represent the shear angles at which intra-ply slip becomes significant

Table 1: Material data overview

		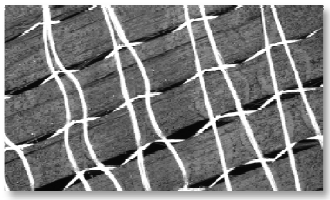
Plain Weave co-mingled Glass/PP	Biaxial Fabric 0/90° - Tricot	Unidirectional carbon fabric
FiberGlass	SAERTEX GmbH & Co. KG	SAERTEX GmbH & Co. KG
TPP60N22P-060	S32CB510-00400-T1270-051000	S32CU970-00320-02000-088939
60 % Glass, 40 % PP	Toray T700 50C 12K	Toray T620 50C 12 K
Areal weight 745 g/m²	Areal weight 416 g/m²	Areal weight 333 g/m²
	Areal weight powder ~6 g/m²	Areal weight powder 8 g/m²